



Deformation by design: data-driven approach to predict and modify deformation in thin Ti-6Al-4V sheets using laser peen forming

Siva Teja Sala¹ · Frederic E. Bock¹ · Dominik Pöltl² · Benjamin Klusemann^{1,2} · Norbert Huber^{1,3} · Nikolai Kashaev¹

Received: 15 February 2023 / Accepted: 9 October 2023
© The Author(s) 2023

Abstract

Abstract The precise bending of sheet metal structures is crucial in various industrial and scientific applications, whether to modify deformation in an existing component or to achieve specific shapes. Laser peen forming (LPF) is proven as an innovative forming process for sheet metal applications. LPF involves inducing mechanical shock waves into a specimen that deforms the affected region to a certain desired curvature. The degree of deformation induced after LPF depends on numerous experimental factors such as laser energy, the number of peening sequences, and the thickness of the specimen. Consequently, comprehending the complex dependencies and selecting the appropriate set of LPF process parameters for application as a forming or correction process is crucial. The main objective of the present work is the development of a data-driven approach to predict the deformation obtained from LPF for various process parameters. Artificial neural network (ANN) was trained, validated, and tested based on experimental data. The deformation obtained from LPF is successfully predicted by the trained ANN. A novel process planning approach is developed to demonstrate the usability of ANN predictions to obtain the desired deformation in a treated region. The successful application of this approach is demonstrated on three benchmark cases for thin Ti-6Al-4V sheets, such as deformation in one direction, bi-directional deformation, and modification of an existing deformation in pre-bent specimens via LPF.

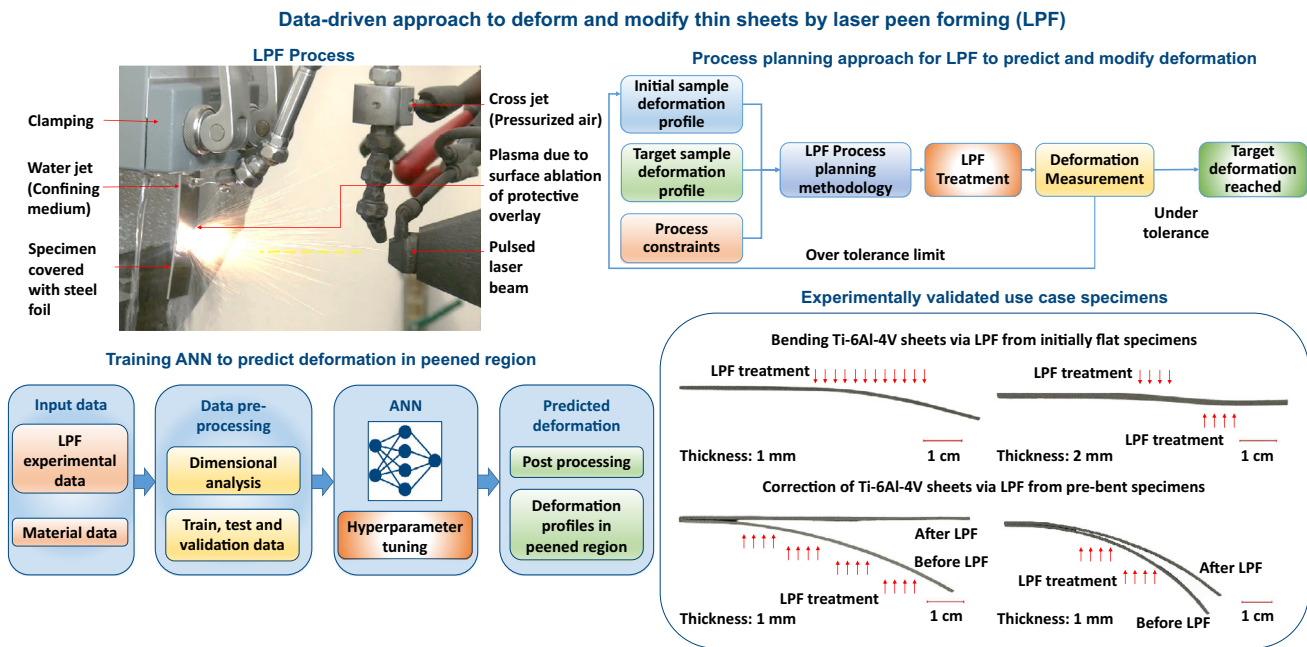
✉ Siva Teja Sala
siva.sala@hereon.de

¹ Institute of Materials Mechanics, Helmholtz-Zentrum Hereon, Max-Planck Str. 1, 21502 Geesthacht, Germany

² Institute for Production Technology and Systems, Leuphana University of Lüneburg, Universitätsallee 1, 21335 Lüneburg, Germany

³ Institute of Materials Physics and Technology, Hamburg University of Technology, Eißendorfer Straße 42, 21073 Hamburg, Germany

Graphical abstract



Keywords Laser peen forming (LPF) · Artificial neural networks · Machine learning · Dimensional analysis · Process planning

Introduction

Sheet metal forming is of primary importance in the automotive and aerospace industries due to its inherent flexibility, production rate, affordability, and energy efficiency, as well as the ability to make structural components with complicated geometries and high dimensional accuracy. Sheet metal bending and stamping are some of the most widely used forming methods for aluminum alloys as described by Zheng et al. (2018). These technologies have been developed to meet the ever-growing demands of the industry to produce sustainable structural sheet metal components that are compliant with dimensional tolerances as discussed in the work of Thimm et al. (2007). The applicability of these traditional forming technologies is yet limited by the mechanical properties of the material such as high yield strength and Young's modulus as observed in titanium alloys by Beal et al. (2006). General formability is significantly affected by springback behavior, which is studied extensively for aluminum alloys and titanium alloys in the works of Laurent et al. (2011) and Badr et al. (2018), respectively. In contrast to traditional sheet metal forming processes, advanced forming technologies such as shot-peening (Kopp & Schulz, 2002), water jet incremental forming (Li & Yang, 2014), laser heating (Safari et al., 2020), and laser peen forming (LPF) whose advances are summarized by Yocom et al. (2018) evolved during the recent times which are capable of dealing with springback to

certain extent. The extensive review of peen forming methods by Gariépy et al. (2014b) indicates that they can be applied to aluminum alloys, steel, and titanium alloys. To fully utilize these innovative technologies, a thorough comprehension of how processing parameters affect deformation is necessary. Additionally, effective process planning strategies that take into account the material's characteristics must be employed.

LPF is a complex cold working process which involves the use of laser-induced mechanical shockwaves that produce plastic deformation at the top surface of the specimen. LPF can be performed by applying an ablative layer (commonly black tape, aluminum or stainless steel foil, or paints) on the treated region to absorb the short energy pulses from the focused laser beam. The short energy pulse from the laser irradiated on the treated region is absorbed by the ablative layer, thereby burning it to generate plasma. A transparent confining medium (generally water or glass) is necessary to prevent the plasma from expanding which results in directing the shockwaves into the specimen (Peyre & Fabbro, 1995). The specimen at focus of the laser is moved relative to the position of the beam which creates a peening sequence or pattern. The plastic deformation due to the peening in the treated region produce plastic strains which vary along the thickness of the specimen. This distribution of plastic strain is responsible for the deformation direction in the treated region as described in the work of Hu et al. (2010b). LPF is successfully applied to a wide range of materials such as pure

aluminum (Sagisaka et al., 2009; Hu et al., 2010b), aluminum alloy 2024-T351 (Zhou et al., 2018), titanium alloy Ti-6Al-4V (Su et al., 2020; Sala et al., 2022), and glass-reinforced epoxy laminate aluminum composites (Hu et al., 2016). A major advantage of LPF in comparison to traditional forming processes is that the compressive stresses induced at the surface reduce the risk of tensile cracks during the forming process.

LPF is ideal for forming large sheet metal structures with reasonably large bend radii without sudden changes in contour, such as wing skins, as described by Baughman (1984) and Ramati et al. (1999). LPF is best suited for forming geometries, such as planar or cylindrical shapes. It is less effective for forming complex shapes with tight curvatures or sharp corners. A study by Hu et al. (2010a) highlights that as the energy used in the peening process increases, the deformation in the treated region also increases. Furthermore, when peening is performed excessively at higher energies or through repeated sequences, it can result in a change in the direction of deformation. LPF can be performed for a wide range of metallic materials to obtain a desired arc radius or to correct deformations in an existing component. It is crucial to determine the appropriate LPF process parameters to achieve the desired arc radius. When required, peening can be performed on both sides of the specimen, which produces complex, saddle-shaped geometries, as demonstrated in the work of Hu et al. (2019). Other possibilities include peening parallel to the edges of the specimen by clamping one edge to produce significant bending along the span of the specimen due to the introduced bending moment. Compound arc radii can also be achieved for pre-bent plates processed with LPF on the surfaces by implementing a process planning approach as reported by Hu et al. (2020). The utilization of LPF as a forming or correction technology can be achieved through the manipulation of peening energy and sequences in specific regions, thus enabling the deformation of components to conform to a desired arc radii. This can be accomplished through the implementation of a multi-step cyclical approach, consisting of iterative peening and measurement until the target geometry is attained. However, the successful execution of these steps necessitates precise identification of LPF process parameters and the regions that require peening.

The majority of studies investigating the LPF process frequently resort to numerical simulation techniques and experimental validation to establish the impact of process variables on the deformation of peened specimens. However, it should be noted that these numerical techniques are dependent on various assumptions and often entail a significant utilization of computational resources. This is a result of the intricacy of the LPF process, which poses challenges in identifying the physical connections between the process variables and the resulting deformation. Thus, it is imperative to effectively exploit the data obtained from experiments to

establish the optimal set of LPF process variables for achieving a desired bend radius or to execute a correction step utilizing LPF. One of the key advantages of utilizing machine learning (ML) techniques in comparison to numerical simulation methods is the ability to make predictions or decisions without a comprehensive understanding of the underlying system. ML algorithms are able to identify patterns and correlations within data sets, even when such relationships are not explicitly programmed into a numerical simulation. This capability allows for predictions or decisions that are more precise or efficient in nature. Furthermore, ML methods possess the ability to adapt and evolve as new data becomes available, whereas numerical simulations often necessitate explicit updates to the model. In recent times, there has been a rapid progression in computational power and ML tools, which has facilitated the applicability of these tools to the development of manufacturing processes and continuum material mechanics, as highlighted in the works of Weichert et al. (2019) and Bock et al. (2019). The creation of a robust model for such studies necessitates a substantial amount of training data, and the generation of this data through experiments or numerical computational methods entails a considerable effort; nonetheless, Kumar et al. (2018) reported the development of an ML approach utilizing bootstrapped gradient descent constrained by dimensional analysis utilizing the Buckingham's Pi theorem and this approach enables the formation of robust predictive ML models from relatively small datasets.

Applications of ML algorithms to traditional sheet metal forming processes are primarily used for process planning and prediction of non-linear relationships between the design parameters, as summarized in the work of Kashid and Kumar (2013). For sheet metal forming, a frequent use of supervised machine learning schemes such as support vector machines (SVM's), decision trees, Naive Bayes classification, and K-nearest neighbors (KNN's) is observed. The work of Liu et al. (2019) demonstrated the application of SVM's to accurately predict and control springback in case of micro W-bending also known as back bending used to form deep 'U'-shaped profiles. Dib et al. (2019) evaluated the performance of several ML approaches to predict the springback and thinning during sheet metal forming, where multi-layer perceptron (MLP) models were the best in identifying springback. The works of Cheng and Lin (2000) as well as Fetene et al. (2016) report implementation of MLP models to predict the bending in case of laser-assisted forming of 304 stainless steel and aluminum alloy 5052-H2. It was observed that MLP models were able to predict the bending angle accurately for different processing conditions. In case of forming thin sheets of aluminum alloy AA 6082, Guarino et al. (2007) demonstrated the application of artificial neural networks (ANNs) to study the influence of laser process parameters to predict the residual inflection during laser forming. Yet, very few

researches take into account the impacts of material properties paired with process parameters when defining inputs and outputs for ANNs that can generalize the model; hence, this is investigated in the present work.

LPF is an emerging technology that can be applied to a wide range of materials to shape complex profiles, correct geometries, and produce small components with distinct features. Nevertheless, the implementation of LPF at an industrial level presents difficulties in terms of LPF process control, which to date has been restricted by the availability of limited robust analytical modeling techniques and complex simulation methodologies. In this context, the present work aims to effectively utilize experimental and material data for creating a data-driven framework to effectively modify and deform thin sheet structures with reasonably large bend radii, maintaining uniform bending throughout the span, without sudden changes in contour. The objective of this work is to develop an ANN-based model to predict the deformation in the peened region after LPF, in case of Ti-6Al-4V sheets of 1 mm and 2 mm in thickness. LPF experiments are performed by varying process parameters such as laser energy, number of peening sequences, and thickness of the specimen. The deformation obtained in the peened region for a particular set of process parameters is measured accordingly. A dataset is to be formulated with LPF process parameters and their corresponding deformations in the peened region respectively. The purpose of this dataset is to be used to train an ANN to make predictions of the deformations in the peened region. Following the collection of experimental data, the physical quantities associated with process parameters and deformations must be transformed into dimensionless Pi-terms using Buckingham's Pi theorem, which will serve as inputs and outputs for the ANN, potentially enhancing the generalization of the model. Once the prediction metrics computed from the output of the ANN model suggest sufficient precision and generalization, the model can be used for the prediction of bending in the LPF-treated region of thin sheets.

In order to effectively correct a pre-deformed shape to a desired target shape, it is essential to possess a thorough comprehension of the LPF process parameters that will generate the necessary deformation. This constitutes an inverse problem, the resolution of which leads to multiple solutions as there can be various permutations of LPF process parameters that could yield identical deformation. To achieve this objective of correction via LPF, a cyclic peen-and-measure process planning methodology is formulated by taking into account all potential combinations of LPF process parameters within the defined parameter space, utilizing the deformation predictions of the trained ANN and certain process constraints. This proposed approach is experimentally validated on test specimens. These test case samples encompass challenges such as bending profiles with varying arc radii, creating 'S'-shaped profiles, modification and complete flattening of

curved regions to achieve a target profile. The experimentally obtained deformation profiles are compared with the target profiles, after being peened with the process parameters obtained from the process planning methodology. This process is repeated until the desired deformation is reached within the tolerance limits corresponding to the target deformation.

Materials and methods

LPF experimental setup

The experimental setup used for the present work (see process video in Sala (2023)) is shown in Fig. 1. LPF was performed using an Nd:YAG laser producing a beam with a square cross-section of 1 mm^2 at focus. The energy distribution of the laser is constant over the region of the laser shot. The laser energy can be varied from 0.1 J to a maximum of 5.0 J. The shape of the laser pulse is a Gaussian profile with a full-width at half maximum (FWHM) of 20 ns. The specimen is rotated around the X-axis to an angle of 25° to avoid damage to the optical system of the laser due to back reflection. The spot size of each laser spot is thus $1.1 \times 1 \text{ mm}^2$. Sheets of 1 mm and 2 mm thick commercial grade AMS 4911 Ti-6Al-4V were used in this study. The size of the LPF specimens is $80 \times 20 \text{ mm}^2$ and the peened region measures $20 \times 20 \text{ mm}^2$. A stainless steel foil of $50 \text{ }\mu\text{m}$ thickness was used as a sacrificial overlay. A stream of water jet is employed to produce a laminar water flow over the specimen which acts as a transparent overlay. The specimen is moved relative to the laser beam to produce the peening pattern as shown in Fig. 1. The varied process parameters considered in this study are summarized in Table 1. A total of 52 experiments (ref. Fig. 12) were performed with various process parameter combinations respectively. A set of 32 experimental process parameter combinations were obtained by considering a general full factorial design encompassing the entire parameter space. The remaining experiments are chosen randomly such that they lie within the defined parameter space.

The deformation in the peened region obtained after LPF was measured using a non-contact linear displacement optical laser triangulation sensor (optoNCDT 2300). A deformation profile is defined as a curve that appears on the section plane vertical to the surface of the sample along the width (see Fig. 2) and obtained by averaging measurements over the span of the specimen at five equidistant positions along the width. The observed standard deviation of averaged deformation values is diminutive (as seen in the error bars of the exemplary specimen in Fig. 2) indicating a uniform bending across the width of the specimen. The margin of error in measured deformation is reduced by fitting a second-order polynomial to the measured data and using the deformation

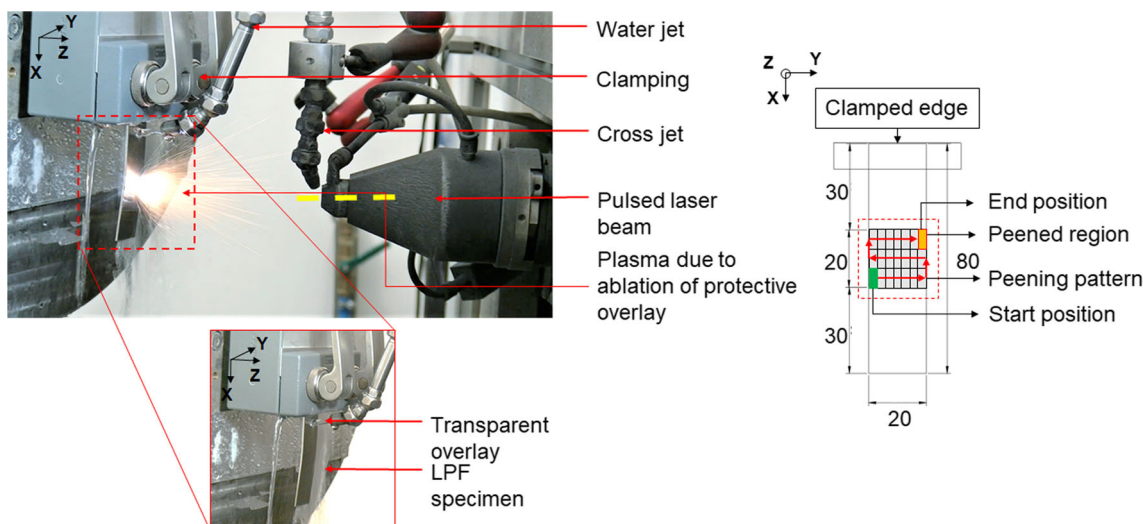


Fig. 1 Experimental setup of LPF process where the LPF specimen is covered with a sacrificial overlay and with a laminar flow of water as a transparent overlay. One edge of the specimen is clamped and the specimen moves relative to the laser beam generating, a zig-zag peening pattern (Color figure online)

values from the fitted function. The obtained deformation profile is rotated by applying a coordinate transformation to ensure that the fixed end remains horizontal (see Fig. 2).

Artificial neural networks

ANNs are emerging abstract computational tools inspired by replicating the functionality of biological neurons. ANNs can be implemented to develop an understanding of various forms of complex data to map containing trends and patterns. The simplest form of an ANN is known as a perceptron, which contains a single input layer and an output node as described by McCulloch and Pitts (1943). In the present work, a fully connected, feed-forward neural network is used that consists of a multiple-layer perceptron model with an input layer, one or more hidden layers,¹ and an output layer. In a feed-forward network, the outputs of one layer are fed as inputs into another layer in the forward direction from inputs to outputs. A mathematical formulation of a feed-forward ANN is described below.

Assuming there are n number of inputs represented by a vector \mathbf{I} (Eq. 1). Hence, the input layer is:

$$\mathbf{I} = [i_1, i_2, i_3, \dots, i_n]. \tag{1}$$

If this neural network comprises p_1, p_2, \dots, p_k units within each of its k hidden layers, the vector representations of these outputs, as denoted by h_1, h_2, \dots, h_k , possess dimensionality that aligns with p_1 through p_k . Consequently, the quantity

¹ The number of hidden layers were determined during hyperparameter tuning of the ANN.

Table 1 LPF process parameters varied in this study

	Process parameter	Range	Unit
1	Laser energy	1.8–3.1	J
2	Number of peening sequences	1–4	–
3	Specimen thickness	1, 2	mm

of units within each layer is referred to as the dimensionality of that specific layer. Then, the weights of connections from the input layer to the 1st hidden layer (h_1 , in Eq. 2) are represented by matrix \mathbf{W}_1 whose size is $n \times p_1$ in the form of:

$$h_1 = f(\mathbf{W}_1^T \mathbf{I}), \tag{2}$$

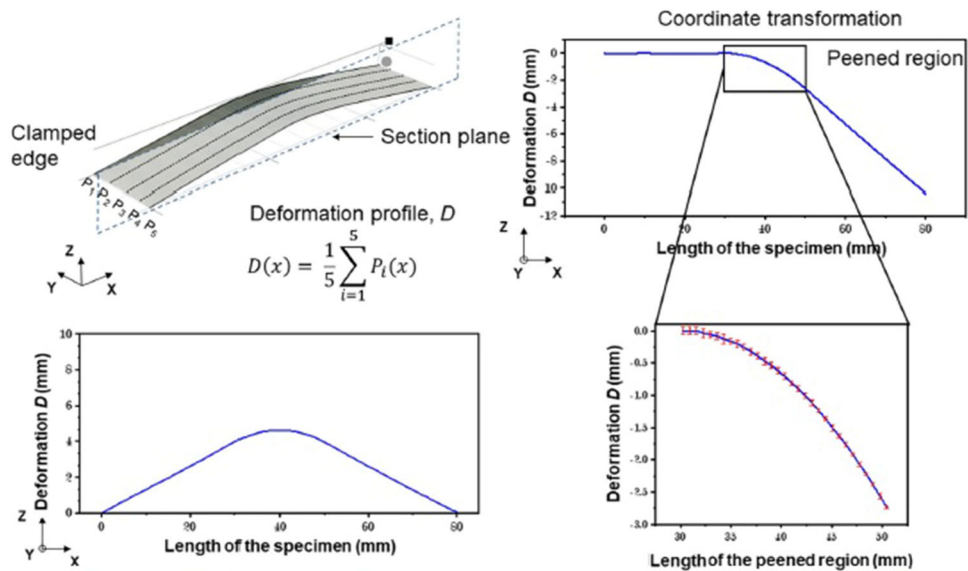
where, f is a non-linear activation function. Similarly, the weights between the r th hidden layer and the $(r + 1)$ th hidden layer are denoted by the matrix denoted by \mathbf{W}_r with the dimensionality of $p_r \times p_{r+1}$. The recursive equation of input from r th hidden layer to $(r + 1)$ th hidden layer can be formulated as:

$$h_{p+1} = f(\mathbf{W}_{p+1}^T h_p) \quad \forall p \in \{1, 2, \dots, k - 1\}. \tag{3}$$

If the number of outputs (m) are denoted by a vector \mathbf{Y} , then the corresponding output layer contains m nodes and the final matrix \mathbf{W}_{k+1} has a dimension of $p_k \times m$ which can be represented as:

$$\mathbf{Y} = [y_1, y_2, y_3, \dots, y_m] = g(\mathbf{W}_{k+1}^T h_k). \tag{4}$$

Fig. 2 Measuring the deformation after LPF for an exemplary specimen: The graph shows the measured and averaged deformation profile (D) over the length of the specimen. A coordinate transformation is applied to rotate the profile such that the fixed end is parallel to the X -axis. The standard deviation of the averaged deformation profile in the peened region ($x = 30.0$ to 50.0 mm) is represented by the error bars in red (Color figure online)



where, g is a linear activation function of the output layer in case of regression tasks.

ANNs can be trained to predict any non-linear relationships between inputs and outputs by adjusting the weights to minimize an error function using the back propagation algorithm described by Rumelhart et al. (1986). Initially, a training instance, or also known as batch size, which is the number of samples from the training dataset, is fed into the neural network which results in forward computations across the layers using an initial set of weights. Then, the back propagation algorithm uses the chain rule of differentials to compute the error gradients as sum of local gradient products of different connections from a node to the output. Finally, the weights corresponding to individual neurons of the ANN are adjusted in such a way that the computed error is minimized. This can be done by controlling the learning rate of the ANN, which is a crucial tuning parameter that controls the step size at each iteration when moving towards a minimum in the loss function. An adaptive learning rate is implemented using available optimizer's such as Adam from a popular open-source Python implementation from Chollet (2015). Finally, the ANN is trained with all the available instances from the training dataset. The weights at each neuron are iteratively adjusted to minimize the error in prediction and a model with best weights is retained at the end of the training process.

The performance of the ANN largely depends on the amount and quality of data on which it is trained, validated, and tested. Nevertheless, it is crucial that the ANN does not overfit the data. A widely used method called *Early Stopping* is elaborately discussed in the work of Yao et al. (2007), which controls the number of iterations based on a specified performance criterion (i.e. mean squared error (MSE)). During each training iteration, the resulting prediction per-

formance is evaluated using a validation dataset (strictly unknown to the ANN). Early stopping is triggered when the performance criterion is fulfilled on the validation dataset, which stops the training process and restores the best weights obtained. In addition to this, it is important to understand the influence of variables or hyperparameters that determine the architecture of the ANN on performance and generalization. In this work, hyperparameters such as number of hidden layers, number of neurons in each hidden layer, learning rate, and type of activation function were varied simultaneously with the aid of random-search-based Python implementations from O'Malley et al. (2019).

Model performance was assessed by the mean squared error (MSE) and the determination coefficient (R^2) which are defined as:

$$\text{MSE} = \frac{1}{n} \left\{ \sum_{i=1}^N (y_i - \hat{y}_i)^2 \right\}, \quad (5)$$

$$R^2 = 1 - \frac{\sum_{i=1}^N (y_i - \hat{y}_i)^2}{\sum_{i=1}^N (y_i - \bar{y})^2}, \quad (6)$$

where, y_i represents the true value, \hat{y}_i is the predicted value and \bar{y} is the mean of true values. The parameter N is the size of the dataset. These statistical indicators were computed based on model predictions versus the true values corresponding to training, validation, and testing datasets.

Data preparation

Data preparation is an important requirement and represents a mandatory pre-processing step. This step helps in the reduction of modeling errors, enhances prediction performance, and leads to overall simplification of the ANN. Koval (2018)

highlighted the importance of a data preparation step and discussed different approaches of dealing with numerical, ordinal, and categorical datatypes. Yet, it is still challenging to select the appropriate input features that efficiently encapsulate the entire properties of interest with limited availability of experimental and physics-based numerical data. Narendra et al. (2019) addressed the challenges of choosing the right set of input parameters for building physically meaningful machine learning models. The work of Huber et al. (2002) demonstrated a hybrid scheme by making use of Buckingham's Pi theorem and by empirically scaling relations between inputs and outputs to predict the material properties of thin film substrates. The studies of Huber and Tsakmakis (2001) as well as Bock et al. (2021) demonstrated that physical normalization of inputs and outputs according to Buckingham's Pi theorem can enhance ANN predictions by reducing prediction errors and increasing the generalization of the model. As a result, for developing a data-driven model, physical quantities involved in LPF, such as process parameters, material constants, and derived variables from material constants are identified and used to achieve physical normalization of inputs and outputs (see Fig. 3).

Considered LPF process-related parameters that are primarily varied are laser energy (E_L), number of peening sequences (n), and thickness of the LPF specimen (T) since they have a higher influence on the deformation in the treated region (Sala et al. (2022)) as well as other experimental process parameters (however not varied) such as the area of cross-section of the focused laser beam (A_f) and duration of the laser pulse (τ). Material parameters, namely Young's modulus (E), density (ρ), and the wave speed ($C = \sqrt{E/\rho}$, which is a measure of the speed of transverse propagation of shockwaves through the thickness of the specimen during LPF) are considered to encapsulate the material related effects into the developed ANN model. The output obtained by varying the process parameters is the deformation profile $D(x)$ in the peened region. Incorporating other process variables and material properties is essential, as they may exert a greater influence on deformation when processing different materials. This comprehensive approach takes into account all factors that impact deformation within the treated area, enhancing the model's robustness and generalizability. By considering these additional variables, the model becomes capable of generating predictions across a wide spectrum of materials and processing conditions, provided it is appropriately trained with relevant data.

After defining these inputs and outputs for the LPF process, one can proceed with developing an ANN model; however, this technique is not particularly an efficient approach because the correlations between the processing parameters, material constants, and other derived parameters are not taken into account. This is clearly evident from the work of Bock et al. (2021). Based on the physical quantities and material

constants, a dimensional analysis is performed with the corresponding input–output parameters to create dimensionless inputs and outputs.

Dimensional analysis can be performed by using Buckingham's Pi theorem which states that if a physically meaningful relationship k_1 involving n number of variables (such as P_1, P_2, \dots, P_n) exists in the form:

$$k_1(P_1, P_2, \dots, P_n) = 0, \quad (7)$$

with a minimum number of fundamental dimensions m to describe those variables, then they can be grouped into $(n - m)$ dimensionless groups referred as π groups in a relation k_2 such that,

$$k_2(\pi_1, \pi_2, \dots, \pi_{(n-m)}) = 0. \quad (8)$$

The dimensionless terms can be formulated as products of parameters (P_i) governing the physical model. A simple formulation of a π -term can be written in the form of:

$$\pi_{ij} = \prod_{i=1}^{(n-m)} P_i^{\alpha_j}, \quad (9)$$

with α_i in \mathbb{N}_0 , where \mathbb{N}_0 is a set of natural numbers. The application of Buckingham's Pi theorem for the experimental process parameters results in the formulation of π -terms as described below:

$$h\left(\frac{ET^3}{E_L}, n, \frac{D}{T}, \frac{T^5\rho}{E_L\tau^2}, \frac{A_f}{T^2}, \frac{C\tau}{T}\right) = 0, \quad (10)$$

and it reflects fundamental physical relationships between experimental process parameters, material properties and deformation after peening. The deformation in the peened region after LPF is measured as profile (see Fig. 2); hence, the nature of the deformation data is a continuous function $D(x)$ over the span of the peened region. It is discretized into 41 points starting from $D(30.0)$ to $D(50.0)$ at equal intervals of 0.5 mm as described as:

$$D = [d(x_j)] \quad \forall j \in [0, 40], \quad (11)$$

where $d(x_j)$ is the deformation at j th position along the length of the peened region. For predicting each deformation value in a deformation profile D , the ANN is provided with information regarding the position j , corresponding to the deformation value $d(x_j)$ and i is the total number of experiments in the parameter space. The formulated dimensionless input space of the ANN model consisting of the experimental

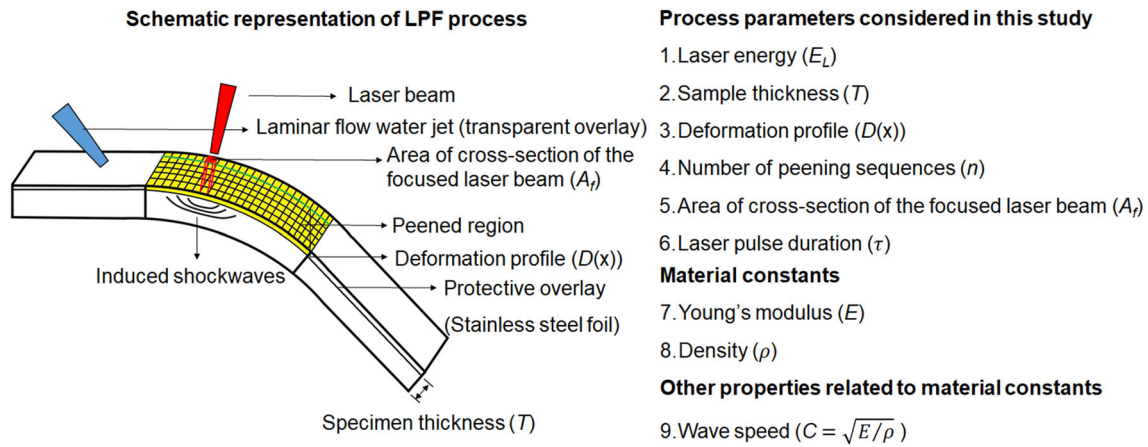


Fig. 3 Schematic representation of the LPF process and a list of governing experimental process parameters and material constants. The material constants and derived quantities are additional features that provide relevant physical information to the model (Color figure online)

data is described as follows:

$$X^{ij} := \left\{ \frac{ET_i^3}{E_L^i}, n_i, \frac{T_i^5 \rho}{E_L^i \tau^2}, \frac{A_f^i}{T_i^2}, \frac{C\tau}{T_i}, \frac{j}{41} \right\}, \quad (12)$$

whereas the output is defined as:

$$Y^{ij} := \left\{ \frac{d^i(x_j)}{T_i} \right\}. \quad (13)$$

Similar approaches of considering an index or positional parameter as an input to ANN were employed in the works of Bock et al. (2021) for predicting induced residual stress profiles after laser shock peening as well as Huber and Tsakmakis (2001) for solving an inverse problem to identify material parameters assessing the viscoplastic behavior, which resulted in good prediction performance.

Overall, the dimensionless input space from experimental data consisted of 52 experiments, with a discretization of 41; therefore, the total number of unique input/output tuples for the ANN are 2132 (i.e. 52×41) which correspond to the global dataset. This data is split into training, validation, and testing datasets with a ratio of 70/15/15. The ANN was trained using 1476 data tuples corresponding to 36 experiments that span across the design space. The validation and testing datasets comprise 328 data tuples each corresponding to 16 experiments within the experimental design space.

To maintain the shape of the original data distribution while setting a specific value range, which is beneficial when the data contains outliers or differs in scale, min-max scaling was applied to both inputs and outputs, scaling them to fall within the range of $[-1, 1]$. This normalization process helps the ANN to effectively learn from the data and maintain numerical stability during training. This scaling procedure was achieved using the following equations:

$$V_{std} = \left\{ \frac{V - v_{min}}{v_{max} - v_{min}} \right\}, \quad (14a)$$

$$V_s = V_{std}(V_{max} - V_{min}) + V_{min}, \quad (14b)$$

where V_s represents the scaled value of the input or output, V is the original value, v_{min} and v_{max} are the minimum and maximum values in the scaled entity, V_{max} and V_{min} are the maximum and minimum values in the feature range. (available in scikit-learn library ref. Pedregosa et al. (2011) as *MinMaxScaler*).

Hyperparameter tuning of ANN

The typical hyperparameters of an ANN are the number of neurons, the number of hidden layers, the learning rate, batch size, and the number of epochs as well as the type of activation functions and the kind of optimizer. In this work, the ANN is trained with experimental data and comprises two hidden layers with a sigmoid activation function¹ and six neurons in each layer. The output layer of the ANN is activated by a linear activation function since the predicted output is a continuous value (Eq. 13). The mean squared error (MSE) is used as the loss function and considered as a metric to evaluate the performance of the model during training. The MSE is minimized gradually by adapting the weights of the ANN using the gradient descent optimization approach which iteratively calculates the local minimum of a differentiable convex function and is one of the most widely used black-box optimizers as described in the work of Ruder (2016). An adaptive learning rate is used to improve the training performance by using the Adam optimizer with a learning rate set to 0.001, while other parameters of the optimizer are set to default values (Kingma & Ba, 2014). Since the dataset is small, the batch size is set to 1; thus, weight updating is performed after each sample is presented to the ANN. The number of epochs is set

to 1000. Over-fitting of the model is prevented by setting up an early stopping trigger to monitor the model performance during training with a patience value of 250 epochs and with a minimum tolerable improvement (δ) of 10^{-3} . Patience is the number of epochs without improvement of prediction metric on the validation set after which the training process gets terminated and δ is the minimum change in MSE to be accounted for improvement of the model i.e. an absolute value of MSE for two consecutive epochs less than δ will count as no improvement. In the present study, ANN implementation is achieved in a Python framework with the aid of open-source libraries Scikit-learn and Keras (Pedregosa et al., 2011; Chollet, 2015).

Data-driven approach for LPF process planning

The process planning of LPF requires solving an inverse problem to find the process parameters that are required to achieve the desired deformation in the peened region. An inverse problem leads to multiple solutions as there can be multiple combinations of LPF process parameters which could result in producing identical deformation. The work of Hu et al. (2020) proposed a combined numerical and experimental process planning strategy by utilizing eigenmoment as an intermediate variable that correlates LPF process parameters to describe deformation obtained after LPF. The proposed strategy was applied to form a saddle-shaped target geometry. The goal of this study is to develop a process planning strategy based on predictions from the trained ANN and apply it to accomplish one-dimensional bending and correction for thin sheets using LPF; thereby, eliminating the need for additional numerical simulations. The multiple solutions can be minimized by defining a set of reasonable process conditions that are influenced by experimental process parameters such as laser energy and the number of peening sequences in the peened regions. For instance, depending on the application, it might be required to limit the number of peening sequences to preserve the surface integrity of the specimen. On the other hand, it could be desired to conduct a peening operation with lower laser energy to achieve precise correction. In these cases, it is required to adapt the process planning of LPF to recognize the importance of such physical constraints.

In this work, a data-driven process planning approach is demonstrated (see Fig. 4) to a number of applications where it is required to achieve a target profile from flat specimens or from specimens already possessing a certain shape. The main objective of this approach is to utilize the predicted deformation values by the trained ANN while considering certain process constraints. The proposed workflow consists of an initial profile, a target profile, a trained ANN, an optimizer and input process constraints, respectively, and their functionalities are described below.

An ANN is trained to predict the deformation in the peened region with certain combinations of experimental parameters within the process parameter space. The trained ANN is validated using a validation dataset and tested against a strictly unknown test dataset. This resulted in a trained ANN that can predict the deformation in the peened region given a combination of process and material parameters i.e. laser energy, number of peening sequences, and thickness of the specimen. A database of all possible process parameter combinations is formulated within the limits of the parameter space corresponding to the training dataset. As a result, a deformation profile corresponding to each unique process parameter combination is predicted by the ANN, and a database of deformation profiles for all possible parameter combinations is generated.

The initial profile (D_i) and target profile (D_t) measured over the span of the specimen (x) to be processed are obtained as shown in Fig. 4. The deviation in deformation between the initial and target profiles is computed as $\Delta D(x) = D_i(x) - D_t(x)$ representing the difference that should be corrected by LPF to achieve the target profile. The $\Delta D(x)$ profile is then discretized into smaller units along the span of the specimen which is essential to identify existing local deformations or curvatures. The length of the discretization step (D_s) is chosen depending on the nature of $\Delta D(x)$ profile and; hence, depends on the complexity of the peened profile. Intuitively, the discretization step size is not constrained to be a constant value and must be adjusted accordingly.

When peening specimens with compound curvatures, a constant value of D_s is suitable; however, peening structures with complex curvatures require varying discretization step sizes over the span. After discretization of the ΔD profile into ' k ' parts, each discretized part of size $D_{s,k}$ (see Fig. 5) can be represented mathematically as shown below:

$$\Delta D_k(x) := \{x, \Delta D(x)\}, \forall x \in [D_{s,(k-1)}, D_{s,k}]. \quad (15)$$

Each discretized part $\Delta D_k(x)$ of the ΔD profile represents the local difference of deformation between the initial and target deformation profiles that should be corrected by LPF. For each discretized unit ' k ', the $\Delta D_k(x)$ profile is approximated with a circular fitting function to obtain the arc radius (R_k) as shown in Fig. 5.

This is accomplished by implementing the least squares fitting method of circles to the discretized data (i.e. $\{x, \Delta D(x)\}$) for ' k ' discretized units, as outlined in the work of Chernov and Lesort (2003). A circular fit is selected as it has been observed that all predicted deformation profiles can be effectively approximated by a circular arc. Fitting a circular arc for the discretized $\Delta D_k(x)$ profiles yields corresponding arc radii R_k , as illustrated in Fig. 5. The arc radius (R_k) is used to construct a deformation profile ($D_k(x_j)$) as shown below:

Fig. 4 Flowchart of the data-driven LPF process planning, showing the integration of ANN-based predictions for peening complex profiles to obtain the target profile geometry. The first step is to obtain the deformation profiles of the initial specimen shape and of the target deformation. The ΔD profile, which is the difference of the two profiles, is calculated. The ΔD profile is discretized into different parts and the corresponding arc radius of each part is computed. Using the arc radius as a key, the optimizer is able to find the process parameters that result in the relevant deformation profiles by taking into account external process restrictions. A peen-and-measure cycle is performed to reduce ΔD to obtain the required target deformation within the desired tolerance level (Color figure online)

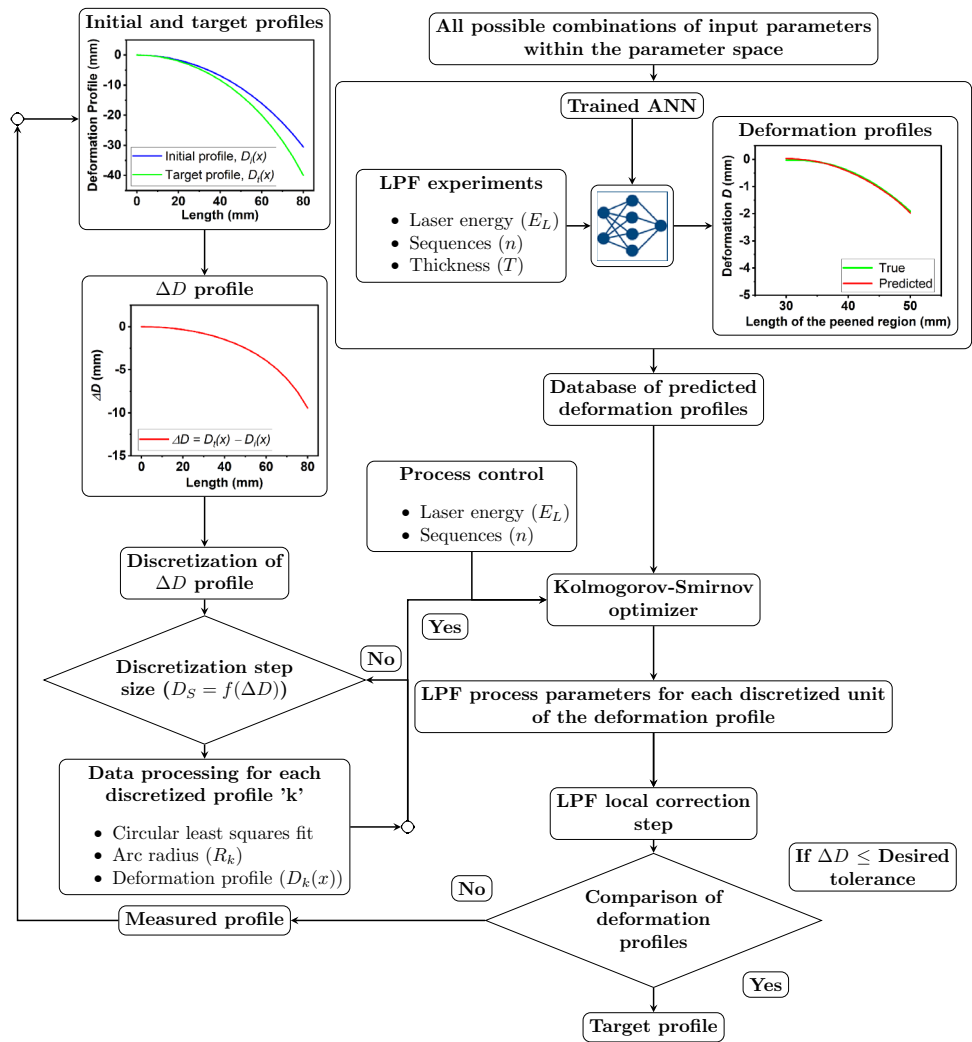
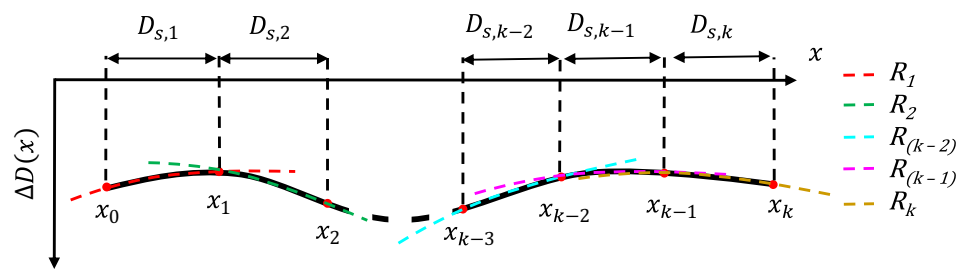


Fig. 5 Discretization of the ΔD profile i.e. $(\Delta D(x) = D_i(x) - D_t(x))$, where, D_i is the initial profile and D_t is the target profile, $D_{s,k}$ is the discretization step size of the k th part of the profile (Color figure online)



$$\Delta D_k(x_j) = \begin{cases} -R_k - \sqrt{R_k^2 - x_j^2} & \text{if } \Delta D_k(x_j) \leq 0 \\ -R_k + \sqrt{R_k^2 - x_j^2} & \text{if } \Delta D_k(x_j) \geq 0. \end{cases} \quad (16)$$

where x_j is the position along the length of the peened region, and is comparable to the predicted output by the ANN trained in this study. As a result, the discretized $\Delta D_k(x)$ profiles are transformed into interpretable deformation profiles.

Reasonably chosen, the discretization of the $\Delta D(x)$ profile allows for peening realistic target shapes without further optimization. However, employing an excessively small dis-

cretization step size can introduce deviations from the desired profile due to accumulated errors, and it tends to escalate the number of processing steps required (ref. Fig. 8b). Conversely, opting for an excessively large discretization step size may lead to erroneous interpretations, particularly when approximating by means of a circular fit. Ideally, the discretization step size (D_s) should be adaptable to the characteristics of the $\Delta D(x)$ profile, as it tends to vary depending on the specific profile under consideration. The current approach for process planning utilizes an iterative

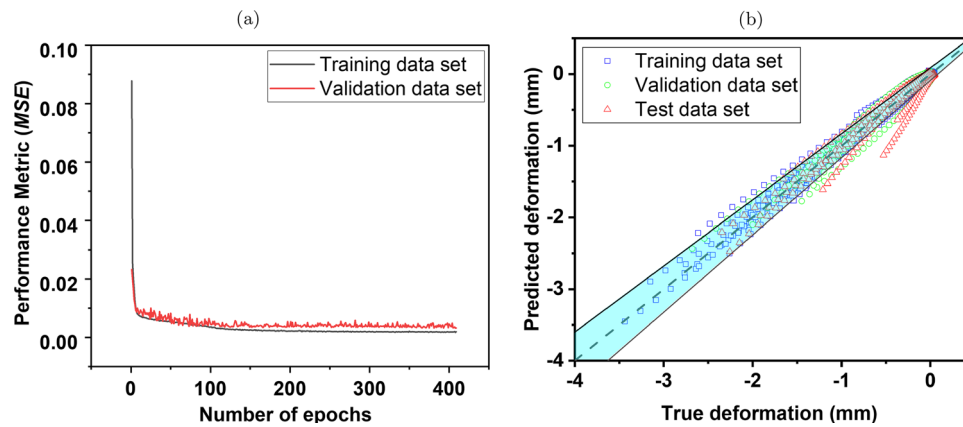


Fig. 6 Performance of the ANN based on the experimental dataset. **a** Performance metric (*MSE*) during training on both training and validation datasets. **b** visualization of predicted deformation values over true deformation values from the trained ANN corresponding to training,

validation, and test datasets. The dashed line signifies that the predicted value is equal to the true value. The conical shaded region represents a relative error of $\pm 10\%$ deviation from the true value (Color figure online)

method, where the number and the length of discretization are strategically determined based on the characteristics of the $\Delta D(x)$ profile, with the goal of minimizing the number of segments and maximizing the length of each segment. The general context for selecting the size $D_{s,k}$ of the k^{th} discretized part of the ΔD profile, aims for larger discretization step sizes whenever feasible. This recommendation ensures optimal processing due to a combination of factors, most notably its ability to significantly reduce processing time by minimizing the required peening cycles. In doing so, it not only enhances operational efficiency but also contributes substantially to conserving energy resources.

During the first iteration, each discretized part of the deformation profile is approximated by a circular fitting function as explained above. The discretization step size for a part of the deformation profile is assessed depending on the quality of fit using the R^2 value (set to be greater than 0.99) and the arc radius of the fit. The arc radius of the fit corresponding to each discretized unit should lie within the minimum and maximum achievable arc radii in the defined process parameter space. A large value of arc radius indicates that the region is flat and does not require any LPF treatment; however, it could also mean that the discretization step size is too small and the deformation profile should be analyzed again by increasing the size of the discretization step. In these circumstances, the discretization step size for each segment is manually modified in small increments until a satisfactory fit is obtained and the arc radius remains within the desired limits. This iterative approach is beneficial as the number of discretizations and length corresponding to each unit can be adjusted to reduce the processing steps. The processed deformation data and corresponding fit data is fed as input to the optimizer on successful discretization of the $\Delta D(x)$ profile.

The optimizer, based on the two-sample Kolmogorov-Smirnov (KS) test as outlined by Simard and L'Ecuyer (2011) and implemented using the Scipy library (Virtanen et al., 2020), is utilized to evaluate whether the approximated $D_k(x)$ profiles align with the ANN predicted deformation profiles within the database. A two-sample KS test is performed for each discretized profile and deformation profile from the predicted database. It is possible that the KS test may yield multiple matches of the $D_k(x)$ from the database of predicted deformation profiles, as various process parameter combinations may lead to the same deformation. Nevertheless, such cases can be avoided by constraining the search criterion based on physical and process constraints. For instance, a physical constraint can be formulated from the database of deformation profiles ($D(x)$) that can be filtered depending on the input process parameter such as the thickness (T) of the material peened. In the present work, LPF process constraints refer to limitations or boundaries that must be adhered to, in order for the process to function correctly and produce reliable deformation in the treated region. The current study has certain limitations for the process, namely, the laser energy must not exceed 3.0 J and the number of peening sequences must be limited to four. This is because using more laser energy causes damage to the sacrificial overlay, and increasing the peening sequences over four does not result in significant additional deformation in Ti-6Al-4V sheets, as reported in the work of Sala et al. (2022). For practical applications, it could be desired to have operational process parameter constraints such as the laser energy (E_L) and the number of sequences (n), which can further reduce the occurrence of multiple matches of $D_k(x)$. The optimizer returns an index of the deformation profile from the database that matches with the formulated deformation profile ($D_k(x)$). The index is used as a key to identify the

Table 2 Performance metrics of the trained ANN on experimental datasets

Dataset	Performance metrics	
	R^2 in %	MSE (mm ²)
Train	97.95	0.04758
Validation	93.95	0.07101
Test	88.99	0.08183

corresponding process parameters. Through this methodology, a suggested set of LPF process parameters is obtained for each discretized profile as an output from the optimizer.

LPF treatment is performed with the output process parameters from the optimizer corresponding to each discretized unit k of the ΔD profile. The deformation profile of the LPF-treated specimen is compared with the target deformation profile. The target profile is successfully achieved by LPF treatment if the deformation profile of the treated specimen lies within a defined tolerance limit of $\pm 10\%$ of the desired target deformation.

Results and discussion

Performance of ANN trained on experimental data

The findings from the ANN trained with the experimental data are discussed in this section. During training, the performance metric (i.e. MSE) was computed on both the training and validation datasets after each epoch. The graph obtained by plotting the performance metric from training data and validation data over the number of epochs is known as the learning curve. The learning curves are extensively used to understand the evolution of the model during training and model behaviors namely an underfit or overfit as well as the representative suitability of the training and validation datasets can be diagnosed using the shape and dynamics of a learning curve. The resulting learning curve of this ANN is shown in Fig. 6a. It can be observed that the MSE reduces and converges as the training progresses, signifying that further training is no longer required.

The training is terminated at 409 epochs and because of the patience of 250 epochs, the optimal weights of the model from epoch 159 are restored due to the early stopping trigger. The performance of the ANN after training is shown in Fig. 6b. It can be observed that the majority of predicted deformation values from the training, validation, and test datasets lie within the $\pm 10\%$ range. Yet, a few outlier values are found in predicting the test data. Overall, the values of R^2 and the MSE , as shown in Table. 2, indicate acceptable agreement between predicted and true deformations on training, validation, and test datasets.

The scatter plot shown in Fig. 6b indicates true versus predicted data from the ANN. The ability of the ANN to generalize can be evaluated based on its performance on the test dataset. The achieved coefficient of determination for the test dataset is 88.9 %. The true deformation profile in the peened region is compared with the predicted deformation from the trained ANN. A reasonable agreement between the true and predicted deformation profile can be observed for the exemplary cases from the test dataset as shown in Fig. 7a–d. In cases where the deformation after LPF is below 1 mm (as in Fig. 7b), it was observed that the predicted deformation from the ANN is higher than the measured deformation. Nevertheless, for significant deformations greater than 1 mm, the predicted profiles show insignificant deviations from the true deformation observed in the experiments.

From the results above, it can be observed that ANN can effectively predict the deformation in the peened region. Yet, these results must be effectively implemented in solving complex use cases. Typical use case applications of LPF involve introducing deformations in a flat specimen or correction of deformations in specimens which might occur due to different processing conditions (Gariépy et al., 2014b). For this reason, a data-driven planning framework is proposed in the present work to demonstrate the application of deformation predictions after LPF, using an ANN trained on experimental data, to modify and deform thin Ti-6Al-4V sheets to obtain desired target shapes.

Application of process planning approach to deform and modify thin sheets

LPF can be performed on large structures with challenging geometries having different curvatures. The desired target deformation can be achieved by using multiple laser energies over different regions of the specimen. In the present work, the proposed data-driven process planning methodology uses the deformation predictions from the trained ANN and aims to modify deformation via LPF without solving an inverse problem. The iterative discretization, optimizer defined by physical and process constraints together presents the flexibility to tailor the process planning strategy to applications with different initial deformation profiles. Additionally, a peen-and-measure cycle reduces the need for redundant LPF treatments.

Hence, the presented process planning approach is tested for four different use cases. The first two use cases demonstrate the applicability of LPF on flat sheets to produce desired target deformation whereas the latter use cases show the modification of a pre-bent structure. In all cases, the process control constraints of the optimizer were set to the possible maximum laser energy ($E_L \leq 3.0$ J) and the number of sequences (n) was less than four due to the process constraints (ref. Sect.. 2.3). The thickness (T) of the sheet

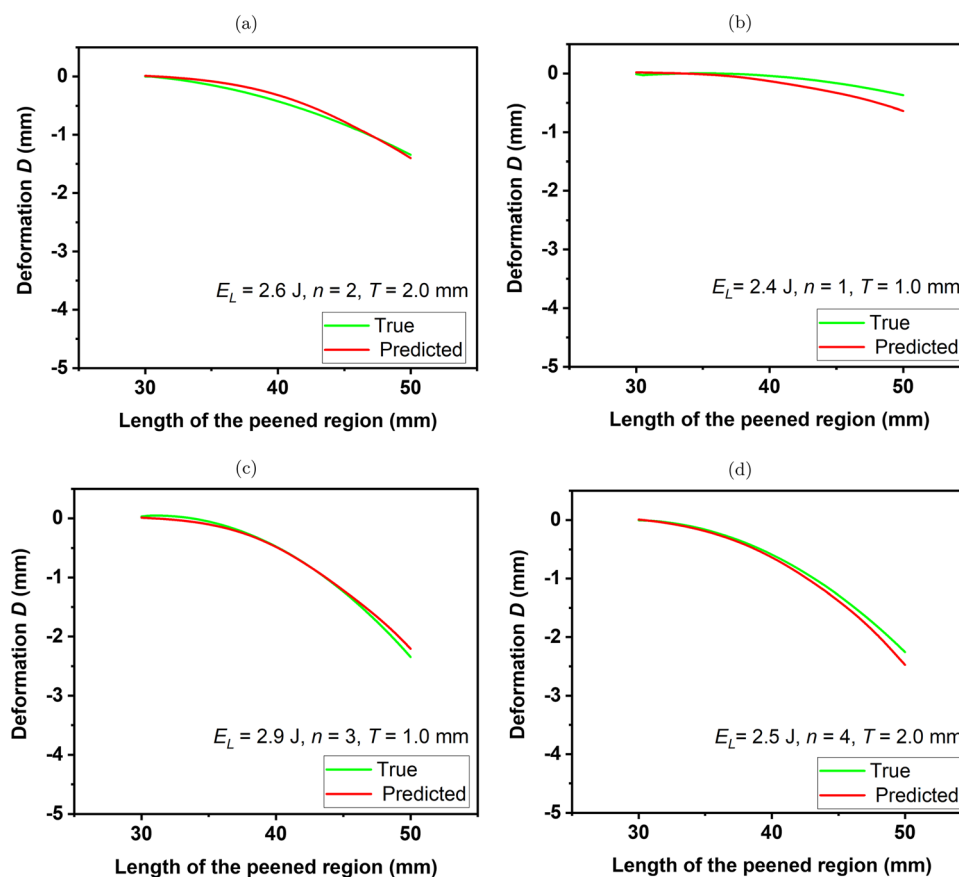


Fig. 7 Comparison of exemplary true vs. predicted deformation values in the peened region generated for various process parameters corresponding to the test dataset which is strictly unknown to the trained ANN. The process parameters E_L is the laser energy, n is the number

material was changed according to the specimen thicknesses used.

Deformation in flat sheets via LPF

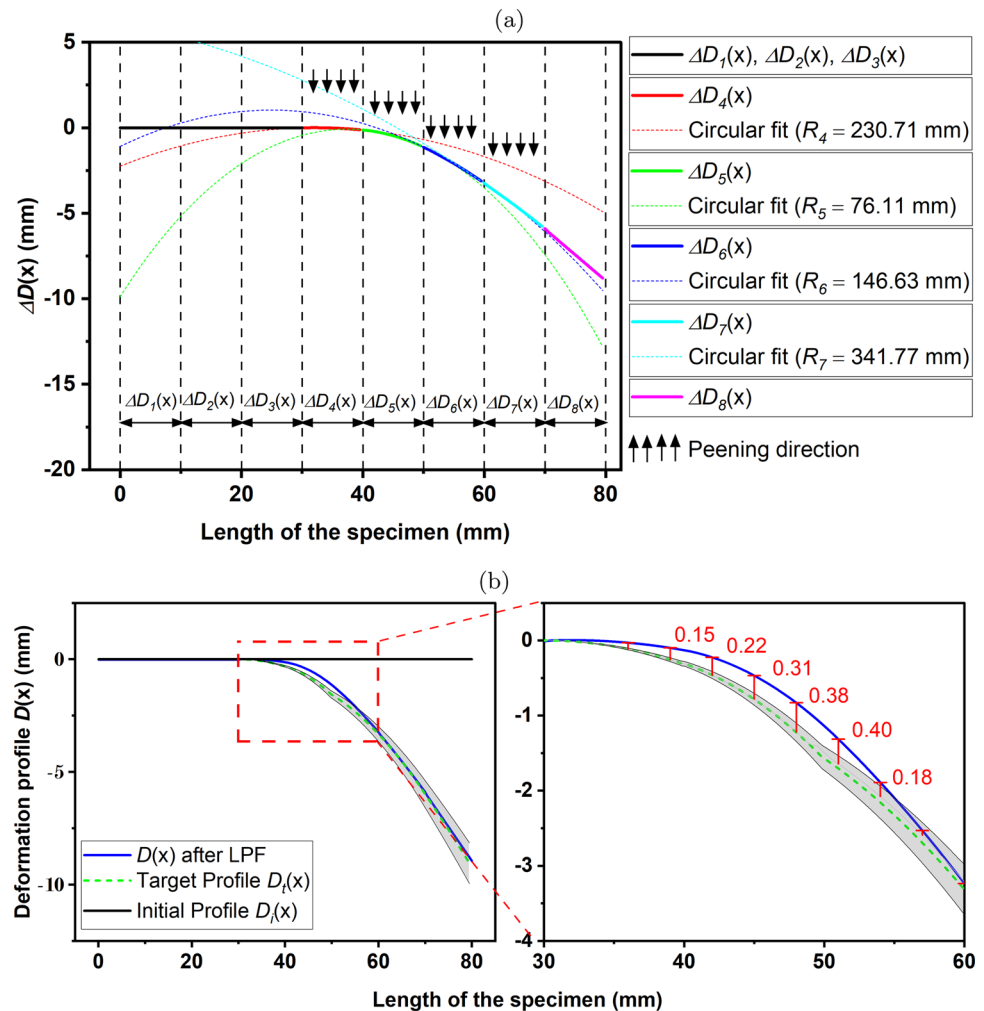
The first use case demonstrates the direct application of LPF treatment at different locations on the flat specimen to reach a desired target deformation for a Ti-6Al-4V sheet that is 1 mm in thickness and 80 mm in length. The ΔD curve corresponding to the initial specimen before peening and target profile was computed. As seen in Fig. 8a, a discretization step size of 10 mm is chosen. The discretized parts $\Delta D_1(x)$, $\Delta D_2(x)$, $\Delta D_3(x)$ and $\Delta D_8(x)$ were not treated as they remained flat, i.e. they correspond to a radius beyond the upper limit of the prediction database of the ANN. The regions of the specimen corresponding to the remaining discretized units were peened with LPF process parameters (E_L , n) suggested by the optimizer (ref. Table 3 in Appendix A) based on the fit with the ANN predicted profiles. A cyclic peen-and-measure cycle as described in Fig. 4 was implemented. The compar-

ison of the deformation profile after the LPF with the target profile (see Fig. 8b) indicates that, a good agreement between the treated and desired profiles achieved using the proposed process planning strategy.

of sequences and T is the thickness of the specimen. The true profile is obtained from real experiments and the predicted profile is the output of the ANN (Color figure online)

After performing four peen and measure cycles over all discretized units, a maximum deviation of 0.40 mm from the target deformation value was observed on the specimen at a distance of 50 mm from the left edge of the specimen, which arises from the predicted deformation values of the ANN. The treated region of the specimen, as shown in Fig. 8, indicate deviations varying from 0.15 mm to 0.4 mm. It is evident from the performance curves of the ANN (depicted in Fig. 6b) that, the expected error in prediction of deformation can reach a maximum of ± 0.5 mm. As the optimizer compares the $\Delta D_k(x)$ profiles after discretization with predicted deformation profiles from the ANN, it results in the mapping of LPF process parameters accordingly. Nevertheless, there could be differences in the predicted deformation and experimentally obtained deformation after LPF treatment which is the potential cause of the observed deviation. Further treatment was

Fig. 8 Use case 1: demonstration of process planning for peening a 1 mm thick flat Ti-6Al-4V specimen to a target profile using the predictions from the trained ANN. **a** Discretization of ΔD profile with a step size of 10 mm. The circular fit data of each discretization is used to reconstruct the deformation profile and is then compared with the database of predicted deformation profiles to obtain the corresponding LPF process parameters. **b** Comparison of the achieved deformation profile and the target profile after LPF treatment at various regions. The grey shaded region indicates a relative error of $\pm 10\%$ deviation from the target deformation (Color figure online)



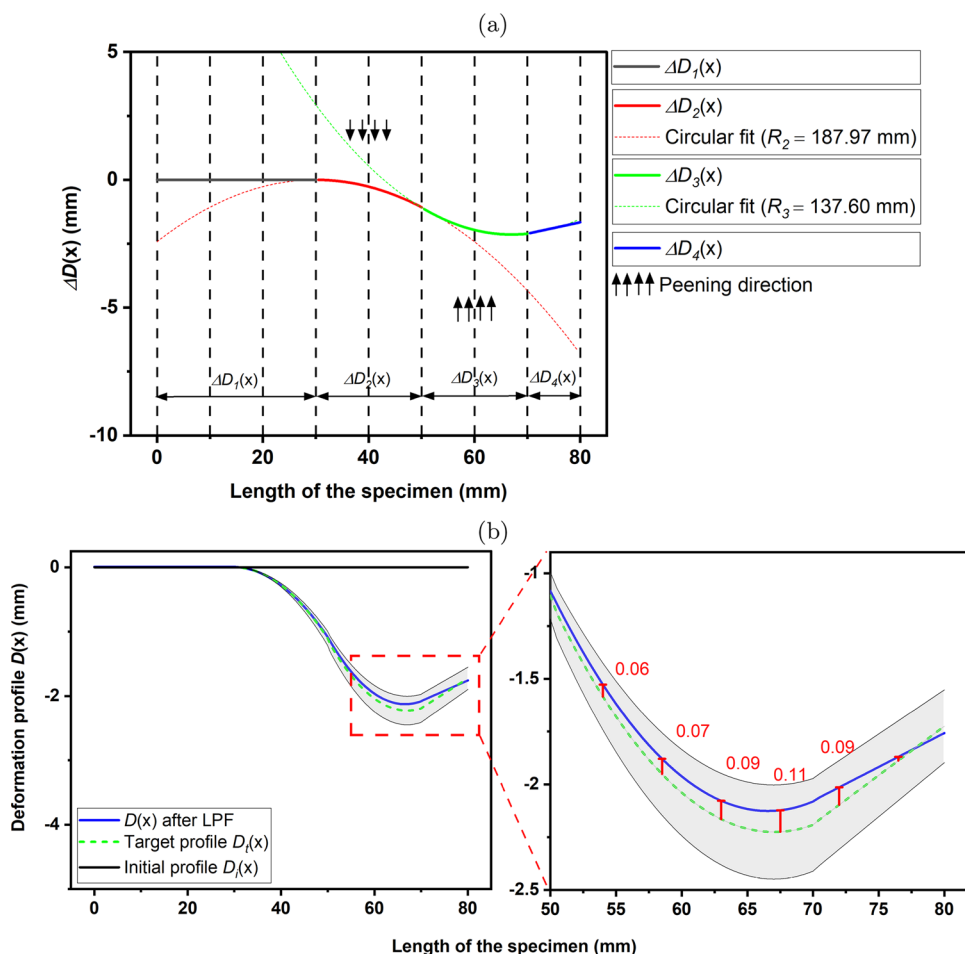
not performed since the difference of the profile after LPF treatment and the target profile resulted in $\Delta D(x)$ profile that upon fitting resulted in an arc radius which is larger than the arc radii corresponding to the deformation profiles of the parameter space. This use case specimen proves that LPF can be applied, to deform thin sheet structures precisely to target shapes with varying curvatures along the span.

True flexibility offered by LPF can be seen when peening both sides of the specimen. As observed in the work of Takeshi et al. (2002) in the case of shot peening, when both sides of a panel are peened with the same energy, the material merely elongates because the bending moments counterbalance each other. Nevertheless, the direction of bending can be changed from convex to concave, i.e. as a saddle or twisted shape, by peening on both sides in different regions by varying LPF process parameters, as demonstrated in the work of Hu et al. (2016). In this regard, another crucial application is, therefore, to be able to obtain more complex shapes via LPF such as ‘S’-shaped curved specimens as shown in Fig. 9a. For demonstrating such an application, a target profile similar to such geometry was considered. In this case, a 2 mm thick flat

Ti-6Al-4V specimen was used and it was peened with ANN-predicted process parameters to obtain a target (‘S’-shaped) deformation profile.

A variable discretization step size (D_s) is chosen to effectively account for the changes in curvature of the target deformation profile. Relying on the fact that the $\Delta D(x)$ profile consists of flat regions and regions with changes in direction of bending from convex to concave, a minimum of four discretizations $\Delta D_1(x)$, $\Delta D_2(x)$, $\Delta D_3(x)$, and $\Delta D_4(x)$ are considered, respectively. To obtain a change in curvature, the specimen was peened on both sides with the predicted process parameters from the trained ANN in the regions corresponding to $\Delta D_2(x)$ and $\Delta D_3(x)$. In the regions $\Delta D_1(x)$ and $\Delta D_4(x)$, was observed that the circular approximation yielded very high values of the arc radii which lie outside the bounds of deformation profiles predicted by the ANN therefore, no LPF treatment was performed. In this case, initially, the region $\Delta D_4(x)$ was peened on one side and the region $\Delta D_3(x)$ was peened on the other side as indicated in Fig. 9a. The deformation profile after LPF treatment is compared with the target profile and it was observed that the

Fig. 9 Use case 2: LPF to obtain an ‘S’-shaped target geometry from a 2 mm thick flat Ti-6Al-4V specimen. **a** A varied discretization step size (D_s) is assumed to effectively peen the specimen. The specimen was peened on both sides at appropriate positions with the LPF process parameters predicted by the ANN. **b** The deformation profile of the LPF-treated specimen is compared with the target profile. A relative error of $\pm 10\%$ deviation from the target shape is shown by the shaded region (Color figure online)



deformation profile $D(x)$ lies within 10% tolerance levels of the desired target profile. The obtained profile after peening precisely agrees with the target profile up to a length of 60 mm (Fig. 9b) and a maximum deviation of 0.11 mm was observed at a length of 67.5 mm. A correction beyond this was not possible since the measured deviation is within the limits of the relative error from the ANN predictions.

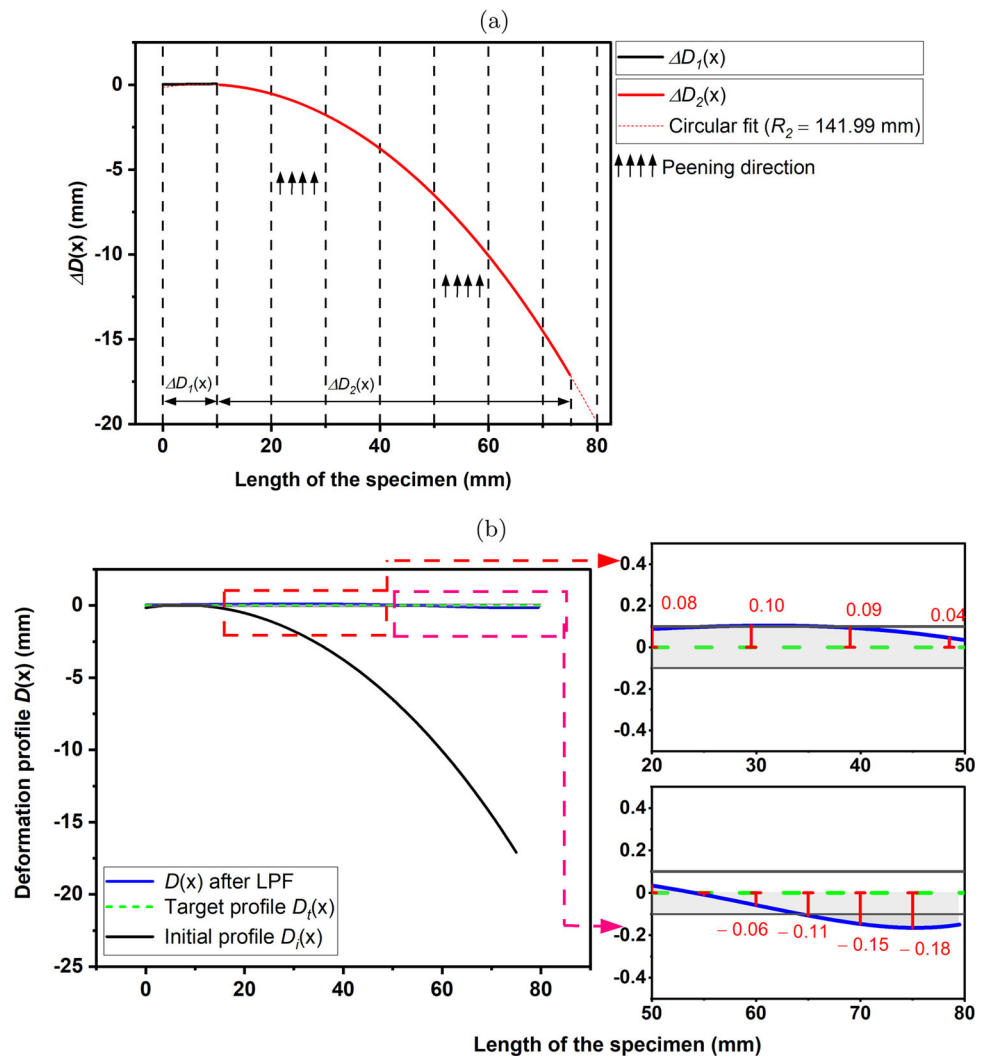
In both the cases of LPF on flat specimens, a convex bending relative to the peening direction was obtained, as the near-surface of the treated region is plastically deformed, and the treated region is bent due to the strain incompatibility between the surface and the remaining region of the specimen (as reported in the work of Hu and Grandhi (2012)). In summary, it can be inferred that the process planning methodology proposed in this study can be utilized to manipulate flat specimens and transform them to attain a predetermined target geometry. To accomplish complex shapes that exhibit a transition in deformation from convex to concave, it is necessary to apply LPF treatment to both sides of the specimen.

Modification of deformation in pre-bent sheets

In addition to being able to form a flat specimen, LPF can also be utilized to precisely correct deformations in pre-bent specimens. This is often necessary for a variety of structural components, as distortions may occur as a result of thermal interactions associated with different manufacturing processes. One example of reshaping with LPF is documented in the work of Friese et al. (2002) in which reshaping was necessary for a laser-welded fuselage of an Airbus A380 aircraft. O’Hara et al. (2002) also reported on the application of peen forming in the case of thin sheets, highlighting the capability of the process to correct deformations. This is particularly appealing for recovering large structural components, as they often represent significant expenses. Therefore, in this work, two use cases were tested to signify the modification of the radius of curvature in pre-bent specimens to a desired target shape by applying the process planning methodology.

To demonstrate a use case of creating a flat specimen by LPF from a bent one, a 1 mm thick Ti-6Al-4V specimen is hand-rolled to obtain a radius of 140 mm that represents the

Fig. 10 Use case 3: flattening of a 1 mm thick Ti-6Al-4V curved specimen of radius 140 mm by LPF treatment using the process parameters derived from the optimizer. **a** Discretization of the ΔD profile into two parts $\Delta D_1(x)$ of 10 mm for the flat region and $\Delta D_2(x)$ of 70 mm in length for the bent region of the specimen. **b** Deviation of the deformation profile from the desired target after LPF treatment over the length of the specimen (Color figure online)



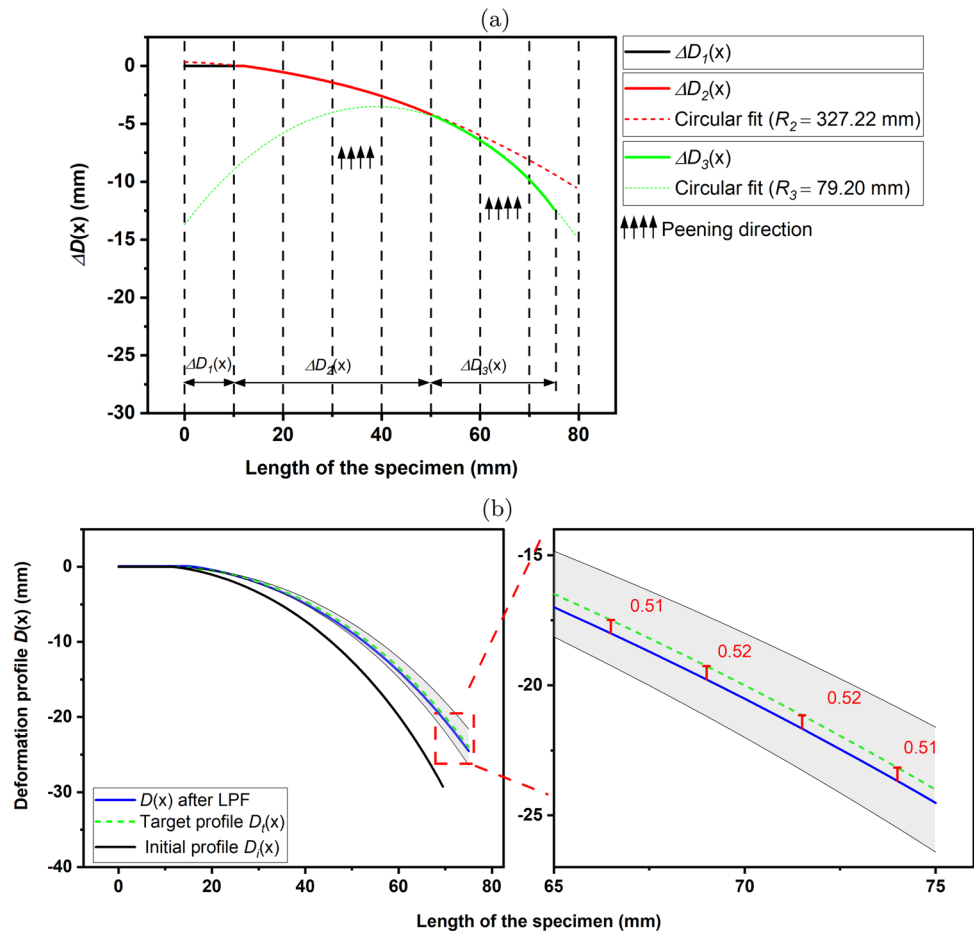
initial deformation of the specimen. This pre-bent specimen is treated locally by LPF using process parameters predicted by the ANN corresponding to each discretized unit. Since $\Delta D(x)$ profile is equal to $D_i(x)$ (as $D_i(x) = 0$ for a flat sample), a discretization step size (D_s) of 65 mm is considered (see Fig. 10a), due to the fact that the arc radius is constant over the entire span of the pre-bent specimen, except the region at the beginning which remained flat. LPF treatment to correct the curvature was applied on the concave region of the specimen to reduce the radius of curvature and to obtain a flat specimen. It was observed that deviations of about 0.10 mm occur in the specimen in between 20 and 50 mm measured from the left edge as shown in Fig. 10b, which lie within the $\pm 10\%$ tolerance level. Yet, larger deviations from the target deformation profile (about -0.18 mm) were observed at both ends of the specimen which might be due to foil delamination during peening (as reported by Sala et al. (2022)). As a result, it can be inferred that pre-bent specimens with constant arc radius can be made entirely flat by successfully

applying LPF; however, a maximum deviation of ± 0.2 mm can occur due to the limitations of the ANN prediction.

LPF can be effectively used to correct small local deviations or errors that may happen during the manufacturing process of curved components. An example of this is when slight adjustments to the arc radius is needed in pre-formed structures or correction of springback during uniform incremental forming of sheet metal structures. Such correction application is demonstrated by considering a 1 mm thick Ti-6Al-4V sheet of 80 mm length that was bent by hand rolling to a radius of curvature of 75 mm; however, a deviation of about 5 mm occurred during the rolling process. A length of approximately 10 mm at the beginning of the specimen was not bent to facilitate clamping.

It was aimed to reduce the radius of curvature to 100 mm by LPF over the span of the specimen except the flat region. Due to the deviation at the right edge of the specimen, during the discretization, it was identified that multiple discretizations are required to correct the curvature of the specimen.

Fig. 11 Use case 4: Application of LPF to correct a curved Ti-6Al-4V sheet with an arc radius of 75 mm to a radius of 100 mm. **a** Computed ΔD profile of the specimen discretized into three parts $\Delta D_1(x)$, $\Delta D_2(x)$ and $\Delta D_3(x)$. The LPF treatment is applied on the concave region of the specimen to reduce the radius of curvature. **b** Comparison of the deformation profile after application of LPF treatment to region $\Delta D_2(x)$ with the target deformation profile. It can be observed that the desired target profile was reached after peening in the region $\Delta D_2(x)$ and; hence, further processing was redundant (Color figure online)



According to the described procedure for discretization, a $\Delta D(x)$ was computed and it was discretized into three parts (see Fig. 11a): $\Delta D_1(x)$ of 10 mm, $\Delta D_2(x)$ of 40 mm and $\Delta D_3(x)$ of 30 mm, respectively. The region $\Delta D_1(x)$ was not treated while $\Delta D_2(x)$ was peened with process parameters returned by the optimizer. The specimen was measured and compared with the target profile. As this is a correction process to reduce the curvature, the discretized unit $\Delta D_2(x)$ from the fixed end was peened first because even small deformations in this region can significantly reduce the deviation at the right edge of the specimen. Besides, peening $\Delta D_3(x)$ first would be counterproductive since it would further decrease the deformation at the edge while treating $\Delta D_2(x)$. After one peen and measure cycle, it was observed that the target deformation profile was achieved, and hence, the region corresponding to $\Delta D_3(x)$ was not peened. The curved region of the specimen with an initial arc radius of 75 mm could be corrected to reach an arc radius of 108 mm after LPF treatment, while the target radius was 110 mm (Fig. 11b). This corresponds to a maximum deviation of 0.51 mm at the free end of the specimen.

Using the database created by the trained ANN, the suggested LPF process planning method can enable successful

deformation of flat and pre-bent specimens by inducing deformations in 1 mm and 2 mm thick sheets, as demonstrated in the use cases above. A cyclic peen-and-measure technique ensures a wide range of process variability, efficiency, and eliminates the need for excessive peening treatments. From the use cases, it was observed that a maximum deviation within $\pm 10\%$ from the desired target might occur and the minimum deformation which can be corrected by LPF is limited by the prediction accuracy of the trained ANN. By taking process control inputs into account, the suggested process planning workflow leads to successful recommendations of LPF process parameters. Nevertheless, it does require critical pre-processing input i.e., discretization step size (D_s) that controls the number of processing steps. As observed in use case 1 (see Fig. 8), very small discretization can result in increased deviations in critical regions. The discretization step size must be selected in such a way that the fitted arc radii (R_k) are not large, which indicate that the discretized unit is flat and does not require LPF treatment. The use cases 1 and 2 demonstrated the applicability of the LPF process to obtain parts with uniform arc radius as well as parts with change in arc radius from convex to concave. On the other hand, the use cases 3 and 4 demonstrated the successful mod-

ification of pre-bent specimens. In these use cases, when the needed $\Delta D(x)$ profile values are less than 0.5 mm, this technique exhibits limitations in suggesting appropriate process parameters as the deformation profile tends to be linear. This might lead to inaccurate conclusions in some instances due to extremely large values of arc radius (R_k) when approximated by a circular fitting function. Nevertheless, significant deformations in thin sheets that are over 0.5 mm can be very precisely corrected or modified to reach a desired target profile.

Conclusions

The current work demonstrates how to precisely form thin Ti-6Al-4V sheets to achieve a certain radius of curvature or to change curvature in pre-bent specimens by LPF utilizing an ANN-based experimental process planning approach. On conducting LPF experiments by varying the process parameters and the material thickness, different deformations in the peened region were observed. For each set of LPF process parameters, the deformation in the peened region was measured along the specimen's length. Yet, the data obtained from the experimental trials could not be used directly; therefore, a data preparation step using Buckingham's Pi theorem was utilized to define the appropriate inputs and outputs to the ANN, improving the generalization of the model and reducing prediction inaccuracies. Various performance measures were used to assess the prediction model's accuracy. The predicted and measured deformations in the peened region of the specimens showed very good agreement, indicating that an ANN model can represent the complicated relationships between the deformation in the peened region and the relevant LPF process parameters without the construction of explicit formulas. As a result, the target deformation is predicted as a part of an LPF planning process by selecting appropriate values for the laser energy and number of peening sequences, which is provided by immediately applying the ANN predictions.

The inverse problem of predicting the LPF process parameters leads to multiple solutions; however, it was observed that by defining a set of physical process constraints, the number of multiple solutions can be limited. A data-driven process planning methodology, utilizing the deformation predictions from the ANN is shown in this study for various applications, where it was necessary to reach a target deformation by LPF. The demonstrated applications involved forming specimens to a desired profile, an 'S'-shaped profile, flattening, and reducing the arc radii of pre-bent specimens. A peen-and-measure cycle was implemented and the initial deformation profile as well as the deformation profile after LPF treatments were compared. The target profile was achieved after repeating the cycle throughout the specimen. This process revealed the importance of choosing appropri-

ate discretization step sizes of the deformation profile. It was observed that for most of the cases, it is required to vary the discretization step size depending on the target deformation. In all cases, upon LPF treatment, the specimens were deformed to reach the target profile within a tolerance level of $\pm 10\%$. The proposed methodology serves as a reliable method for determining the optimal LPF process parameters from a database generated using the predictions of the trained ANN.

Author contributions STS, FEB, NH and NK conceptualized the study; methodology, investigation and visualization was conducted by STS; resources were gathered by NK and BK; STS did the writing - original draft preparation; STS, FEB, DP, NH, BK, and NK did the writing—review and editing; NH and NK supervised the study. All the authors have read and agreed to the published version of the manuscript.

Funding Open Access funding enabled and organized by Projekt DEAL. The work was carried out under the auspices of the PEENCOR project (Project Numbers: 20Q1920C, 20Q1920D), which is funded by the German Federal Ministry of Economic Affairs and Climate Action (BMWK) under the LuFo VI-1 program.

Data availability The dataset used to create the ANN in this study will be provided by the corresponding author upon a reasonable request.

Declarations

Conflict of interest The authors declare no conflict of interest.

Open Access This article is licensed under a Creative Commons Attribution 4.0 International License, which permits use, sharing, adaptation, distribution and reproduction in any medium or format, as long as you give appropriate credit to the original author(s) and the source, provide a link to the Creative Commons licence, and indicate if changes were made. The images or other third party material in this article are included in the article's Creative Commons licence, unless indicated otherwise in a credit line to the material. If material is not included in the article's Creative Commons licence and your intended use is not permitted by statutory regulation or exceeds the permitted use, you will need to obtain permission directly from the copyright holder. To view a copy of this licence, visit <http://creativecommons.org/licenses/by/4.0/>.

Appendix

The data corresponding to all the LPF experiments to train, test and validate the ANN's is illustrated in Fig. 12 below. The varied LPF process parameters are laser energy, number of sequences and the thickness of the specimen. LPF experiments at these data points were performed and their corresponding deformation profiles in the peened region were measured, respectively.

The LPF process parameters corresponding to every discretized unit in each use case returned by the optimizer are tabulated below (Table 3).

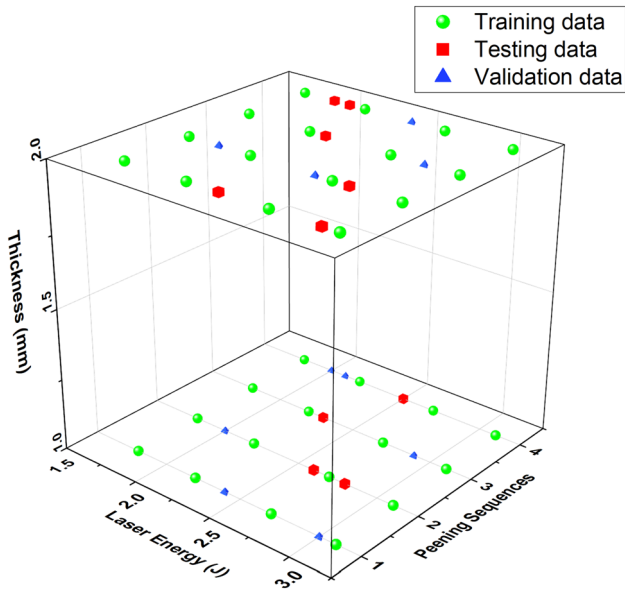


Fig. 12 LPF process parameters considered in this study (Color figure online)

Table 3 List of LPF process parameters suggested by the optimizer for each discretized unit in the use case specimens

Use case	Number of discretized units	Discretized unit	Length of each discretization (mm)	Predicted process parameters by the trained ANN		
1	8	$\Delta D_1(x)$, $\Delta D_2(x)$, $\Delta D_3(x)$	10	Unpeened region		
		$\Delta D_4(x)$	10	$E_L = 1.9J, n = 2$		
		$\Delta D_5(x)$	10	$E_L = 2.4J, n = 4$		
		$\Delta D_6(x)$	10	$E_L = 2.2J, n = 3$		
		$\Delta D_7(x)$	10	$E_L = 2.1J, n = 3$		
		$\Delta D_8(x)$	10	Unpeened region		
		2	4	$\Delta D_1(x)$	30	Unpeened region
				$\Delta D_2(x)$	20	$E_L = 2.0J, n = 4$
$\Delta D_3(x)$	20			$E_L = 1.8J, n = 3$		
$\Delta D_4(x)$	10			Unpeened region		
3	2	$\Delta D_1(x)$	10	Unpeened region		
		$\Delta D_2(x)$	66	$E_L = 2.0J, n = 3$		
4	3	$\Delta D_1(x)$	10	Unpeened region		
		$\Delta D_2(x)$	40	$E_L = 2.2J, n = 1$		
		$\Delta D_3(x)$	25	$E_L = 2.0J, n = 4$		

References

- Badr, O. M., Rolfe, B., & Weiss, M. (2018). Effect of the forming method on part shape quality in cold roll forming high strength Ti–6Al–4V sheet. *Journal of Manufacturing Processes*, 32, 513–521. <https://doi.org/10.1016/j.jmapro.2018.03.022>
- Baughman, D. (1984). An overview of peen forming technology. In *Comprehensive Materials Processing*, pp 28–32. Conf Proc: ISCP–2, Chicago, IL.
- Beal, J. D., Boyer, R., & Sanders, D. (2006). Forming of titanium and titanium alloys. In *Metalworking: Sheet Forming*, pp 656–669. ASM International. <https://doi.org/10.31399/asm.hb.v14b.a0005146>
- Bock, F. E., Aydin, R. C., Cyron, C. J., Huber, N., Kalidindi, S. R., & Klusemann, B. (2019). A review of the application of machine learning and data mining approaches in continuum materials mechanics. *Frontiers in Materials*, 6, 110.
- Bock, F. E., Keller, S., Huber, N., & Klusemann, B. (2021). Hybrid modelling by machine learning corrections of analytical model predictions towards high-fidelity simulation solutions. *Materials*, 14(8), 1883.
- Cheng, P., & Lin, S. (2000). Using neural networks to predict bending angle of sheet metal formed by laser. *Journal of Machine Tools and Manufacture*, 40(8), 1185–1197.
- Chernov, N. & Lesort, C. (2003). Least squares fitting of circles and lines. <https://arxiv.org/abs/cs/0301001> Accessed on 15 June, 2022.
- Chollet, F. et al. (2015). Keras. <https://keras.io>, Accessed on 21 April, 2022.
- Dib, M. A., Oliveira, N. J., Marques, A. E., Fernandes, M. C., Ribeiro, B. M., & Prates, P. A. (2019). Single and ensemble classifiers for defect prediction in sheet metal forming under variability. *Neural Computing and Applications*, 32(16), 12335–12349.
- Fetene, B. N., Shufen, R., & Dixit, U. S. (2016). FEM-based neural network modeling of laser-assisted bending. *Neural Computing and Applications*, 29(6), 69–82.
- Friese, A., Lohmar, J., & Wustefeld, F. (2002). Current applications of advanced peen forming implementation. p. 16–20. Conf Proc: ICSP-8, Garmisch-Partenkirchen.
- Gariépy, A., Miao, H., & Lévesque, M. (2014b). Peen forming. In *Comprehensive Materials Processing*, pp. 295–329. Elsevier.
- Guarino, S., Ucciardello, N., & Tagliaferri, V. (2007). An application of neural network solutions to modeling of diode laser assisted forming process of AA6082 thin sheets. *Key Engineering Materials*, 344, 325–332.
- Hu, Y., & Grandhi, R. V. (2012). Efficient numerical prediction of residual stress and deformation for large-scale laser shock processing using the eigenstrain methodology. *Surface and Coatings Technology*, 206(15), 3374–3385. <https://doi.org/10.1016/j.surfcoat.2012.01.050>
- Hu, Y., Han, Y., Yao, Z., and Hu, J. (2010a). Three-dimensional numerical simulation and experimental study of sheet metal bending by laser peen forming. *Journal of Manufacturing Science and Engineering*, 132(6).
- Hu, Y., Luo, M., Hu, L., & Yao, Z. (2020). Efficient process planning of laser peen forming for complex shaping with distributed eigen-moment. *Journal of Materials Processing Technology*, 279, 116588. <https://doi.org/10.1016/j.jmatprotec.2020.116588>
- Hu, Y., Xi, Y., Wu, D., & Yao, Z. (2019). Quantitative evaluation of specimen geometry effect on bending deformation of laser peen forming. *International Journal of Mechanical Sciences*, 150, 404–410.
- Hu, Y., Xu, X., Yao, Z., and Hu, J. (2010b). Laser peen forming induced two way bending of thin sheet metals and its mechanisms. *Journal of Applied Physics*, 108(7):073117.
- Hu, Y., Zhang, Z., & Yao, Z. (2016). Shape prediction for laser peen forming of fiber metal laminates by experimentally determined eigenstrain. *Journal of Manufacturing Science and Engineering*, 4, 139.
- Huber, N., Nix, W. D., & Gao, H. (2023). Identification of elastic-plastic material parameters from pyramidal indentation of thin films. *Proceedings of the Royal Society of London. Series A*, 458, 1593–1620. <https://doi.org/10.1098/rspa.2001.0927>
- Huber, N., & Tsakmakis, C. (2001). A neural network tool for identifying the material parameters of a finite deformation viscoplasticity model with static recovery. *Computer Methods in Applied Mechanics and Engineering*, 191(3–5), 353–384. [https://doi.org/10.1016/S0045-7825\(01\)00278-x](https://doi.org/10.1016/S0045-7825(01)00278-x)
- Kashid, S., & Kumar, S. (2013). Applications of artificial neural network to sheet metal work: A review. *American Journal of Intelligent Systems*, 2(7), 168–176.
- Kingma, D. P. & Ba, J. (2014). Adam: A method for stochastic optimization. <https://arxiv.org/abs/1412.6980>
- Kopp, R., & Schulz, J. (2002). Flexible sheet forming technology by double-sided simultaneous shot peen forming. *CIRP Annals*, 51(1), 195–198. [https://doi.org/10.1016/S0007-8506\(07\)61498-X](https://doi.org/10.1016/S0007-8506(07)61498-X)
- Koval, S. I. (2018). Data preparation for neural network data analysis. In *2018 IEEE Conference of Russian Young Researchers in Electrical and Electronic Engineering (EIConRus)*, pp. 898–901. <https://doi.org/10.1109/EIConRus.2018.8317233>
- Kumar, N., Rajagopalan, P., Pankajakshan, P., Bhattacharyya, A. S., Balachandran, J., & Waghmare, U. V. (2018). Machine learning constrained with dimensional analysis and scaling laws: Simple, transferable, and interpretable models of materials from small datasets. *Chemistry of Materials*, 31(2), 314–321.
- Laurent, H., Coër, J., Grèze, R., Manach, P. Y., Andrade-Campos, A., Oliveira, M. C., & Menezes, L. F. (2011). Mechanical behaviour and springback study of an aluminium alloy in warm forming conditions. *ISRN Mechanical Engineering*, 2011, 1–9.
- Li, H. & Yang, X. P. (2014). Research on technology of high-pressure water jet incremental sheet metal forming. In *Frontiers of Manufacturing and Design Science IV*, volume 496 of *Applied Mechanics and Materials*, pp. 148–154. Trans Tech Publications Ltd. <https://doi.org/10.4028/www.scientific.net/AMM.496-500.148>
- Liu, X., Du, Y., Lu, X., and Zhao, S. (2019). Springback prediction and forming accuracy control of micro W-bending using support vector machine. In *2019 6th International Conference on Frontiers of Industrial Engineering (ICFIE)*. IEEE.
- McCulloch, W. S., & Pitts, W. (1943). A logical calculus of the ideas immanent in nervous activity. *The Bulletin of Mathematical Biophysics*, 5(4), 115–133.
- Narendra, K., Rajagopalan, P., Pankajakshan, P., Bhattacharyya, A., Sanyal, S., Balachandran, J., & Waghmare, U. V. (2019). Machine learning constrained with dimensional analysis and scaling laws: Simple, transferable, and interpretable models of materials from small datasets. *Chemistry of Materials*, 31(2), 314–321. <https://doi.org/10.1021/acs.chemmater.8b02837>
- O'Hara, P. (2002). Peen-forming - a developing technique. Conf Proc: ICSP-8, Garmisch-Partenkirchen.
- O'Malley, T., Bursztein, E., Long, J., Chollet, F., Jin, H., Invernizzi, L., et al. (2019). Kerastuner. <https://github.com/keras-team/kerastuner>, Accessed on 21 April, 2022.
- Pedregosa, F., Varoquaux, G., Gramfort, A., Michel, V., Thirion, B., Grisel, O., Blondel, M., Prettenhofer, P., Weiss, R., Dubourg, V., Vanderplas, J., Passos, A., Cournapeau, D., Brucher, M., Perrot, M., & Duchesnay, E. (2011). Scikit-learn: Machine learning in Python. *Journal of Machine Learning Research*, 12, 2825–2830.

- Peyre, P., & Fabbro, R. (1995). Laser shock processing: A review of the physics and applications. *Optical and Quantum Electronics*, 27(12), 1213–1229. <https://doi.org/10.1007/BF00326477>
- Ramati, S., Levasseur, G., & Kennerknecht, S. (1999). Single piece wing skin utilization via advanced peen forming technology. pp. 28–32. International shot peening conference in Warsaw, Poland (ICSP-7).
- Ruder, S. (2016). An overview of gradient descent optimization algorithms.
- Rumelhart, D. E., Hinton, G. E., & Williams, R. J. (1986). Learning representations by back-propagating errors. *Nature*, 323(6088), 533–536.
- Safari, M., de Sousa, R. A., & Joudaki, J. (2020). Recent advances in the laser forming process: A review. *Metals*, 10(11), 1472.
- Sagisaka, Y., Kamiya, M., Matsuda, M., & Ohta, Y. (2009). Thin-sheet-metal bending by laser peen forming with femtosecond laser. *Journal of the Japan Society for Technology of Plasticity*, 50(584), 868–872.
- Sala, S. T., Keller, S., Chupakhin, S., Pörtl, D., Klusemann, B., & Kashaev, N. (2022). Effect of laser peen forming process parameters on bending and surface quality of Ti-6Al-4V sheets. *Journal of Materials Processing Technology*, 305, 117578.
- Sala, S. T. (2023). Laser peen forming of thin Ti-6Al-4V sheet (Version 2). *figshare*. <https://doi.org/10.6084/m9.figshare.24190731.v2>
- Simard, R., & L'Ecuyer, P. (2011). Computing the two-sided Kolmogorov-Smirnov distribution. *Journal of Statistical Software*, 39(11), 89. <https://doi.org/10.18637/jss.v039.i11>
- Su, B., Wang, H., Cao, Y., Pei, X., & Hua, G. (2020). Local deformation and macro distortion of TC4 titanium alloy during laser shock processing. *The International Journal of Advanced Manufacturing Technology*, 106(11–12), 5421–5428.
- Takeshi, Y., Takayuki, T., Makoto, I., Shuzo, S., & Takahiro, O. (2002). Development of shot peening for wing integral skin for continental business jets. *Mitsubishi Heavy Industries Technical Review*, 39(2), 57–61.
- Thimm, G., Rui, W., & Yongsheng, M. (2007). Tolerance transfer in sheet metal forming. *International Journal of Production Research*, 9(14), 3289–3309.
- Virtanen, P., Gommers, R., Oliphant, T. E., Haberland, M., Reddy, T., Cournapeau, D., Burovski, E., Peterson, P., Weckesser, W., Bright, J., van der Walt, S. J., Brett, M., Wilson, J., Millman, K. J., Mayorov, N., Nelson, A. R. J., Jones, E., Kern, R., & Larson, E. (2020). SciPy 1.0: Fundamental Algorithms for Scientific Computing in Python. *Nature Methods*, 17, 261–272.
- Weichert, D., Link, P., Stoll, A., Rüping, S., Ihlenfeldt, S., & Wrobel, S. (2019). A review of machine learning for the optimization of production processes. *The International Journal of Advanced Manufacturing Technology*, 5–8, 1889–1902.
- Yao, Y., Rosasco, L., & Caponnetto, A. (2007). On early stopping in gradient descent learning. *Constructive Approximation*, 26(2), 289–315. <https://doi.org/10.1007/s00365-006-0663-2>
- Yocom, C. J., Zhang, X., & Liao, Y. (2018). Research and development status of laser peen forming: A review. *Optics and Laser Technology*, 108, 32–45. <https://doi.org/10.1016/j.optlastec.2018.06.032>
- Zheng, K., Politis, D. J., Wang, L., & Lin, J. (2018). A review on forming techniques for manufacturing lightweight complex—shaped aluminium panel components. *International Journal of Lightweight Materials and Manufacture*, 1(2), 55–80.
- Zhou, W. F., Ren, X. D., Wang, C. C., Yang, X. Q., & Larson, E. A. (2018). Residual stress induced convex bending in laser peen formed aluminum alloy. *Journal of Laser Applications*, 30(1), 012001.

Publisher's Note Springer Nature remains neutral with regard to jurisdictional claims in published maps and institutional affiliations.